

Article

# Initial Design of a Novel Barge-Type Floating Offshore Wind Turbine in Shallow Water

Yiming Zhou <sup>1,†</sup>, Sensen Feng <sup>2,†</sup>, Xiaojiang Guo <sup>1</sup>, Feng Tian <sup>3</sup>, Xu Han <sup>2,\*</sup> , Wei Shi <sup>4,5</sup>  and Xin Li <sup>2,\*</sup>

<sup>1</sup> Huaneng Clean Energy Research Institute, Beijing 102209, China

<sup>2</sup> Institute of Earthquake Engineering, Faculty of Infrastructure Engineering, Dalian University of Technology, Dalian 116024, China

<sup>3</sup> Huaneng Guangdong Shantou Offshore Wind Power Co., Ltd., Shantou 515071, China

<sup>4</sup> State Key Laboratory of Coastal and Offshore Engineering, Dalian University of Technology, Dalian 116024, China

<sup>5</sup> Research Institute, Dalian University of Technology in Shenzhen, Shenzhen 518057, China

\* Correspondence: xu.han@dlut.edu.cn (X.H.); lixin@dlut.edu.cn (X.L.)

† These authors contributed equally to this work.

**Abstract:** The studies on floating offshore wind turbines (FOWTs) have been increasing over recent decades due to the growing interest in offshore renewable energy. The present paper proposes a barge platform with four moonpools to support the Technical University of Denmark 10 MW wind turbine for a designed water depth of 60 m. A  $4 \times 2$  mooring system with eight mooring lines is also proposed for the barge platform. The main dimensions of the barge platform are optimally selected with respect to its preliminary hydrodynamic properties and potential financial benefit. The proposed barge-type FOWT is then demonstrated to be aligned with the DNV standard requirements in terms of its intact and damage stability. Furthermore, coupled time-domain simulations are conducted for the proposed barge FOWT with mooring under the selected environmental and operational conditions by using Simo-Riflex-AeroDyn (SRA). Through decay test simulations, the natural periods of the barge-type FOWT are demonstrated to be within the DNV recommended ranges. The proposed mooring system is also benchmarked with the  $3 \times 3$  mooring concept that was used for a 3 MW barge-type FOWT installed in Kitakyushu. The response magnitudes of the barge platform and mooring line tension are similar to both mooring systems, and thus the  $4 \times 2$  mooring system is preferred due to its lower cost. In addition, the proposed barge platform is preliminarily demonstrated to be able to survive for the 50-year extreme environmental conditions under parked wind turbine status, as well as the normal environmental conditions under the operating status.

**Keywords:** floating offshore wind turbine; barge-type platform; stability analysis; fully coupled time-domain simulation; dynamic response



**Citation:** Zhou, Y.; Feng, S.; Guo, X.; Tian, F.; Han, X.; Shi, W.; Li, X. Initial Design of a Novel Barge-Type Floating Offshore Wind Turbine in Shallow Water. *J. Mar. Sci. Eng.* **2023**, *11*, 464. <https://doi.org/10.3390/jmse11030464>

Academic Editors: José António Correia and Giuseppe R. Tomasicchio

Received: 1 December 2022

Revised: 2 February 2023

Accepted: 17 February 2023

Published: 21 February 2023



**Copyright:** © 2023 by the authors. Licensee MDPI, Basel, Switzerland. This article is an open access article distributed under the terms and conditions of the Creative Commons Attribution (CC BY) license (<https://creativecommons.org/licenses/by/4.0/>).

## 1. Introduction

Energy has become a key factor restricting social and economic development. With the increasing focus on sustainability, the vigorous development of renewable energy including wind resources has become an important part of the development strategies for many countries. According to statistics [1,2], the global wind energy is about  $2.74 \times 10^9$  MW, of which the  $2 \times 10^7$  MW available wind energy is 10 times the total water energy that can be developed and used globally. Compared with onshore wind energy, developing offshore wind energy has the advantages of larger reserves, wider distribution, more stable wind speed, and no occupation of land. In addition, offshore wind turbines have less visual and noise pollution than onshore ones. Wind power generation gradually moves from land to sea and from shallow to deep sea to obtain higher energy conversion efficiency. Among the varieties of offshore wind floating platforms [3–6], barge platforms are beneficially characterized by simple structure, easy manufacturing, good stability,

convenient transportation, flexible deployment, and low cost. The barge-type floating wind turbine is better in stability performance due to it being equipped with a very large pontoon and a wider water plane area to obtain the sufficient righting moment.

The barge-type FOWTs' dynamic responses have been broadly researched both numerically and experimentally. Conventional catenary anchor mooring systems have been typically considered for the developed concepts of barge-type FOWTs. National Renewable Energy Laboratory and Massachusetts Institute of Technology proposed a barge-type floating wind turbine concept, focusing on its design, fabrication, and installation [7]. Wayman and Sclavounos [8] presented a coupled dynamic model for the floating wind turbine systems in the frequency domain. Jonkman and Buhl [9] presented fully coupled simulation tools of aero-hydro-servo-elastic and simulated the loads of a 5 MW wind turbine installed on a squared barge-type platform. In extreme wave conditions, they found that the barge platform is sensitive to the excessive pitching. Through fully coupled response analyses, Jonkman and Matha [10] investigated the dynamics of three 5 MW offshore floating wind turbine concepts, including a spar, a tension leg platform (TLP), and a barge. Compared with the land-based system, all the floating wind turbines show increased loads on turbine components, and they must be reinforced. Zhao et al. [11] and Ren et al. [12] analyzed the dynamic response of a novel semi-submersible platform and TLP platform, respectively. The results indicate that the novel semi-submersible FOWT has good stability and the tendon failure conditions lead to the most critical TLP platform dynamic behaviors. A lot of dynamic analyses were performed for each model using the fully coupled time-domain aero-hydro-servo-elastic design code FAST with AeroDyn and HydroDyn. Mayilvahanan and Selvam [13] studied a barge-type floating platforms of different width-to-length ratios from 0.4 to 1.0 and studied the dynamic response under wave and wind loading conditions in the time domain by using the integro-differential equation of motion. The results show that the barge with the width-to-length ratio of 1.0 leads to the smallest pitch RAO but the largest heave RAO at  $0^\circ$ .

In the early 2010s, the concept of the IDEOL floating platform was presented, which has a ring-shaped surface floater with a shallow draught [14]. The platform was equipped with a damping pool structure in the center, improving the entire floating platform and wind turbine stability. The platform motion under the wind and wave loads can be reduced by the coupling from the moonpool. Borisade et al. [15] used the method of multibody system fluid dynamics to investigate the performance of the IDEOL platform and its mooring system by coupled numerical simulation at full scale. Guignier et al. [16] presented a multibody modeling methodology for the global load analysis of FOWT under wave and wind conditions, improving the estimation of the heave added mass. Choynet et al. [17] conducted numerical simulation of two 6 MW IDEOL barge-type wind turbine units in the forms of concrete or steel. It was concluded that the platform material has little impact on its dynamic behavior with the same moonpool width. Kosasih et al. [18] applied the Boundary Element Method (BEM) to simulate the dynamics of a barge-type FOWT including the moonpool and the bottom skirt considering the additional viscous damping. Using BEM to simulate the dynamic behavior of the barge-type FOWT showed a good consistency with the experiment results. Vijay et al. [19] studied the influence of different moonpool forms on the motion of barge-type FOWTs by establishing an aero-hydro-servo-elastic coupling model using FAST. The frequencies of the moonpool sloshing modes becomes higher when the number of moonpools changes from one to four. Ikoma et al. [20] found that a barge with multiple moonpools can improve the hydrodynamic performance of the FOWT compared with the single-moonpool barge-type platform. Ikoma et al. [21] later investigated the response of barge floating systems with four moonpools and vertical-axis wind turbines by applying numerical and experimental approaches. Compared with the single-moonpool structure, the barge-type platform with multiple moonpools may improve the platform's pitch and surge performance. However, multi-moonpool structures may have more complex hydrodynamic phenomena, requiring further analysis and research.

Therefore, the concept of a barge-type FOWT with multiple moonpools is interesting to study in terms of its dynamic behaviors.

The present paper proposes a novel barge-type platform with four moonpools, for a 60 m water depth to support the DTU (Technical University of Denmark) 10 MW reference wind turbine. After briefly introducing the applied theories in Section 2, the design of the barge-type FOWT is depicted in Section 3. The main dimensions of the platform are optimally selected based on the surge force and pitch natural period in the frequency domain. Stability analyses are performed for both the intact and damage conditions are summarized in Section 4. Then, the coupled time-domain simulations are executed for the selected environmental conditions using SIMA [22]. In addition, the dynamic behaviors of the barge-type FOWT with the  $4 \times 2$  mooring system are compared with the  $3 \times 3$  mooring system to investigate the impact of mooring design on the platform dynamics. Furthermore, the optimal mooring system design for the 10 MW barge FOWT is selected. The relevant results are presented in Section 5. Finally, conclusions and summary of future work are given in Section 6.

## 2. Methodology Description

### 2.1. Aerodynamics

The turbine aerodynamic loads can be calculated based on the theory of blade element momentum. A blade is assumed to be divided into many small elements on which the forces can be superimposed along the blade span to calculate the total forces and moments applied on the turbine. Based on the blade element theory [23], the aerodynamic loads on a single blade element can be calculated as follows.

First, the airflow velocity at each element  $V_{rel}$  is calculated by:

$$V_{rel} = \sqrt{(1 - a)^2 V_1^2 + (\Omega r)^2 (1 + b)^2} \tag{1}$$

where  $a$  is the axial induction factor,  $V_1$  is the incoming velocity of airflow,  $b$  is the tangential induction factor,  $\Omega$  is the rotating angular velocity, and  $r$  is the distance between the root of blade and the airfoil section.

The inflow angle  $\theta$  is calculated by:

$$\theta = \arctan \frac{(1 - a)V_1}{(1 + b)(\Omega r)} \tag{2}$$

Then the lift and drag of blade element (i.e.,  $dF_L$  and  $dF_d$ ) is calculated by:

$$dF_L = \frac{1}{2} \rho_a V_{rel}^2 c C_L dr \tag{3}$$

$$dF_d = \frac{1}{2} \rho_a V_{rel}^2 c C_D dr \tag{4}$$

where  $\rho_a$  is the density of the air,  $c$  is the chord of the airfoil. Then the thrust and moment acted on a single blade element, i.e.,  $dT$  and  $dQ$  can be written by:

$$dT = dF_L \csc \theta + dF_d \sin \theta = \frac{1}{2} \rho_a V_{rel}^2 (C_L \cos \theta + C_D \sin \theta) c dr \tag{5}$$

$$dQ = (dF_L \csc \theta - dF_d \sin \theta) r = \frac{1}{2} \rho_a V_{rel}^2 (C_L \sin \theta - C_D \cos \theta) c r dr \tag{6}$$

where  $C_L$  and  $C_D$  are the lift and drag coefficients of the airfoil, respectively.

The unsteady aerodynamics are based on the semi-empirical Beddoes–Leishman dynamic stall model, incorporating the aerodynamic effects of the tip losses, the hub losses, and the skewed wake. In the present study, SIMA was used to fit the aerodynamic part, and we used blade element momentum theory to calculate the aerodynamic loads on the wind turbine including tower.

### 2.2. Hydrodynamics

Even though one may consider using advanced approaches for computational fluid dynamics with high-fidelity models to investigate the detailed wave-induced dynamics of floating structures, this requires competence of selecting suitable numerical algorithm and turbulence models with significantly large computational cost [24]. Therefore, at the stage of initial concept design, linear hydrodynamic theory was applied to estimate the sea loads and barge-type floating platform motions. The response amplitude of the floating platform is therefore assumed to be proportional to the excitation at the same frequency with a phase difference between them.

#### 2.2.1. Governing Equations

The potential theory assumes the fluid flow to be incompressible, inviscid (frictionless), and irrotational. For the completeness of the present paper, the governing equations of the potential theory are briefly described hereafter according to [25].

The fluid velocity can be written as a vector  $V(x, y, z, t) = [u, v, w]^T$ , where  $u, v$ , and  $w$  are the fluid velocity vector in  $x, y$ , and  $z$  directions, respectively. The incompressible flow satisfies:

$$\nabla \cdot V = \frac{\partial u}{\partial x} + \frac{\partial v}{\partial y} + \frac{\partial w}{\partial z} = 0 \tag{7}$$

where  $\nabla$  is the partial derivative operator. In the fluid domain  $\Omega_0$ , as illustrated in Figure 1, the irrotational fluid does not initiate the rotation, i.e.,  $\nabla \times V = 0$ . This means that the velocity vector can be represented by the gradient of a scalar parameter, i.e., the velocity potential  $\phi$ , satisfying:

$$u = \frac{\partial \phi}{\partial x}, v = \frac{\partial \phi}{\partial y}, w = \frac{\partial \phi}{\partial z} \tag{8}$$

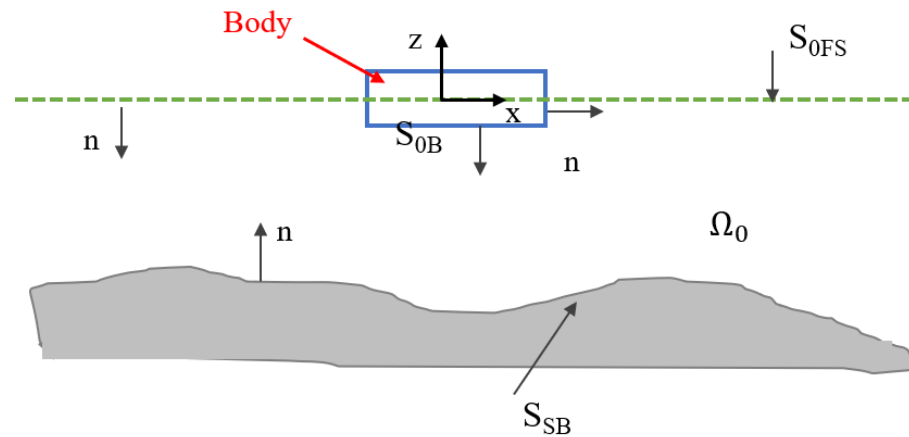


Figure 1. Boundary conditions for linear waves.

Based on Equations (7) and (8), the velocity potential representing fluid motion satisfies the Laplace equation:

$$\frac{\partial^2 \phi}{\partial x^2} + \frac{\partial^2 \phi}{\partial y^2} + \frac{\partial^2 \phi}{\partial z^2} = \nabla^2 \phi = 0 \tag{9}$$

At the sea bottom (i.e.,  $S_{SB}$  as illustrated in Figure 1), the impermeable boundary condition satisfies:

$$\frac{\partial \phi}{\partial n} = 0 \tag{10}$$

The boundary condition at the body wet surface (i.e.,  $S_{0B}$  as illustrated in Figure 1) can be written as:

$$\frac{\partial \phi}{\partial n} = V_B \cdot n \tag{11}$$

where  $V_B$  is the body velocity vector,  $\mathbf{n}$  is the vector perpendicular to the boundary surface pointing outwards. At the free surface (i.e.,  $S_{0FS}$  in Figure 1), it is assumed that the fluid particles remain at the surface and the pressure equals the ambient pressure. These boundary conditions are further simplified by removing the nonlinear terms, leading to:

$$\frac{\partial^2 \phi}{\partial t^2} + g \frac{\partial \phi}{\partial z} = 0 \tag{12}$$

Then, the velocity potential could be calculated according to the aforementioned equations. Consequently, the wave-induced loads on the structure can be calculated by integration of the dynamic pressure around the wet surface estimated from the Bernoulli equation.

### 2.2.2. Equations of Motion

The equation for the rigid body motion of the floating platform can be written by [26]:

$$\sum_{k=1}^{k=6} (M_{jk} + A_{jk}) \ddot{\eta}_k + B_{jk} \dot{\eta}_k + C_{jk} \eta_k = F_j e^{-i\omega_e t} \quad (j = 1, \dots, 6) \tag{13}$$

where  $j$  and  $k$  represent the degree of freedom (DoF),  $j, k \in \{1, 2, 3, 4, 5, 6\}$ .  $M_{jk}$  is an element of the mass matrix  $\mathbf{M}$ ;  $A_{jk}$  is an element of the added mass matrix  $\mathbf{A}$ , representing the added mass in  $j$ th DoF due to a unit acceleration in the  $k$ th DoF;  $B_{jk}$ , in the damping matrix  $\mathbf{B}$ , represents the damping in the  $j$ th DoF due to a unit velocity in the  $k$ th DoF;  $C_{jk}$  in the hydrostatic stiffness matrix  $\mathbf{C}$ , represents the stiffness in the  $j$ th DoF due to a unit displacement in the  $k$ th DoF.  $\ddot{\eta}_k$ ,  $\dot{\eta}_k$ , and  $\eta_k$  are the acceleration, velocity, and displacement of the  $k$ th DoF motion, respectively;  $F_j$  is the force in the DoF  $j$  in the force vector  $\mathbf{F}$ ; and  $e^{-i\omega_e t}$  is the harmonic exponential.

According to potential theory, in the frequency domain, the equation of rigid body motion can be expressed by [27]:

$$(\mathbf{M} + \mathbf{A}(\omega)) \ddot{\boldsymbol{\eta}}(\omega) + \mathbf{B}(\omega) \dot{\boldsymbol{\eta}}(\omega) + \mathbf{C}(\omega) \boldsymbol{\eta}(\omega) = \mathbf{F}(\omega) \tag{14}$$

where  $\mathbf{F}(\omega)$  can represent mooring forces, environmental forces, or other external forces.

For the nonlinear system, the solution to this equation must be solved iteratively in the time domain. By using the Cummins equation, the equation introduces a convolutional integral (Duhamel integral), which is also called the delay function, capable of converting Equation (14) into the time domain

$$(\mathbf{M} + \mathbf{A}_\infty) \ddot{\boldsymbol{\eta}}(t) + \int_0^\infty \mathbf{h}(t - \tau) \dot{\boldsymbol{\eta}}(\tau) d\tau + \mathbf{C} \boldsymbol{\eta}(t) = \mathbf{F}(t) \tag{15}$$

where  $\mathbf{A}_\infty$  is the added mass matrix at the infinite frequency;  $\mathbf{h}(t - \tau)$  is the retardation function;  $\mathbf{F}(t)$  is the external excitation forces, including:

$$\mathbf{F}(t) = \mathbf{F}^{wave}(t) + \mathbf{F}^{wind}(t) + \mathbf{F}^{mooring}(t) \tag{16}$$

where  $\mathbf{F}^{wave}$  is the wave-induced force;  $\mathbf{F}^{wind}$  is the wind-induced force; and  $\mathbf{F}^{mooring}$  is the force induced by mooring system.

## 3. Numerical Model

### 3.1. Design of the Substructure for the 10 MW Wind Turbine

One important objective of the present research is to design a barge platform to support the DTU 10 MW wind turbine for a water depth of 60 m, which is considered to be a representative water depth along China's coastal area. The properties of the DTU 10 MW wind turbine are listed in Table 1 [28].

**Table 1.** Specification of DTU 10 MW wind turbine.

Parameter	Values
Wind Regime	IEC class 1 A
Cut-in wind speed	4.0 m/s
Rated wind speed	11.4 m/s
Cut-out wind speed	25.0 m/s
Rotor diameter	178.3 m
Hub diameter	5.6 m
Hub Height	119.0 m
Minimum rotor speed	6.0 rpm
Maximum rotor speed	9.6 rpm
Maximum tip speed	90.0 m/s
Hub overhang	7.1 m
Shaft tilt angle	5.0 deg
Blade mass	230,667 kg
Nacelle mass	446,036 kg
Tower Mass	591,758 kg

As illustrated in Figure 2, the proposed floating barge has an octagonal shape equipped with a skirt on the bottom to reduce the heave motion of the FOWT inspired by the IDEOL platform [17]. Furthermore, there are retaining walls in the middle of the platform to divide the single moonpool into four. It is worth noting that based on an earlier simple study, the natural periods of the four-moonpool barge tends to favorably increase compared with the single-moonpool barge concept, which is also observed by Vijay et al. [19] for pitch. Consequently, dividing the moonpool into four may unfavorably lead to larger platform motions at larger periods. Therefore, it is important to thoroughly check the platform motions and structural integrity against relevant standards at the initial and detailed design phases. However, comparing the dynamic behaviors of the single- and four-moonpool barge-type FOWTs is considered out of the scope for the present paper.

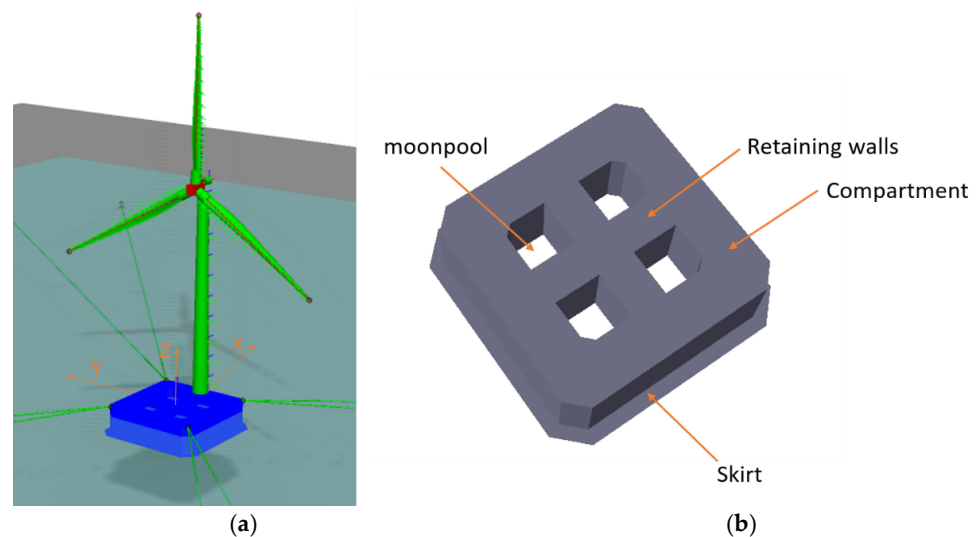


**Figure 2.** Illustration of the proposed barge-type FOWT: (a) sketch of the overall barge-type FOWT with the global coordinate system including wind turbine, barge platform, and mooring system; (b) details of the barge platform.

The coordinate reference system is also shown in Figure 2. The origin is located at the sea level in the center of the platform. The x-axis is perpendicular to the wind turbine rotor swept area and the z-axis is positive pointing upward, as shown in Figure 2a. Wind and wave direction follows the same convention, as illustrated in Figure 3. A wave direction of 0° indicates the wave goes towards the positive x-axis.

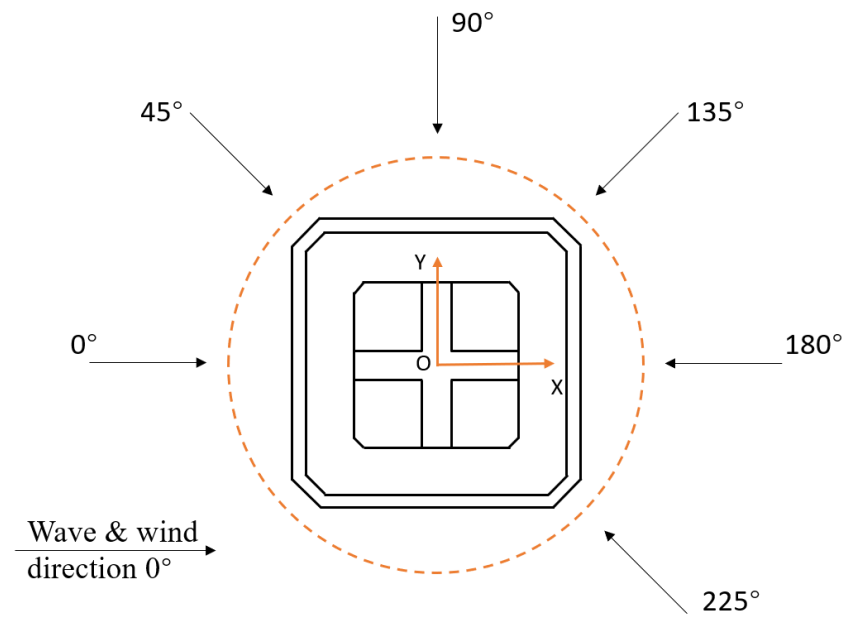


**Figure 3.** Schematic diagram of the direction of wind and wave propagation.

It is critical to decide the dimensions of the platform and main components (i.e., skirt, retaining walls, and compartments) to design it to sufficiently support the DTU 10 MW wind turbine. For a certain water depth, the hydrodynamic performance of the barge platform depends on the dimensions and geometry of the platform. The influence of the key dimensions on the hydrodynamic force in surge and the pitch resonance periods was investigated through a sensitivity study. The considered barge platforms with different sizes are summarized in Table 2, with the same draft of 10 m. Variations in the widths of the platform, compartment, skirt, and retaining walls were considered. The consistency of the draft was ensured by adjusting the inertia distribution of compartment contents. It is worth noting that in comparison with the concept of a semi-submersible platform supporting the DTU 10 MW wind turbine with a draft of 20 m [29], the barge-type platform has a much smaller draft. This could be more suitable for relatively shallow waters, e.g., in water depths of 60 m, where the applications of the floating foundations may be more cost-saving than the fixed foundations for offshore wind turbines [30].

**Table 2.** Main dimensional information about the considered different platforms for the initial selection of the barge (unit: m).

Model ID	Platform Width (Incl. Skirt)	Compartment Width	Skirt Width	Retaining Walls Width
M1	54	10	3	6
M2	56	10	3	6
M3	58	10	3	6
M4	60	10	3	6
M5	60	10	3	7
M6	60	10	3	8
M7	60	11	3	6
M8	60	12	3	6
M9	60.6	10	3.3	6
M10	61	10	3.5	6

The SESAM-HydroD module [31] was applied to obtain the platform RAOs as well as the hydrodynamic coefficients of the barge platform such as the hydrostatic stiffness, additional damping, and added mass coefficients. The first-order excitation forces

per unit wave amplitude in surge and the pitch RAOs for different platform sizes are shown in Figure 4.

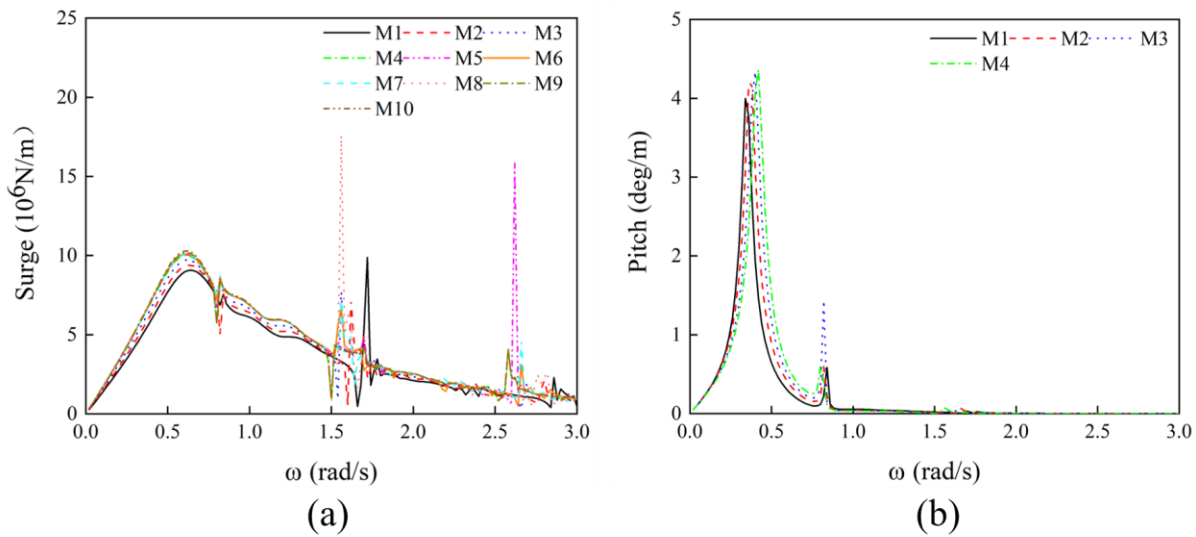


**Figure 4.** Hydrodynamic analysis results: (a) comparison of first-order wave exciting force per unit wave amplitude in surge for various platform dimensions; (b) comparison of pitch RAOs for various platform dimensions.

A total of 10 models with different sizes are shown in Table 2 to obtain the optimal platform motion performance. The wave frequencies between 0.02 rad/s and 3 rad/s with the interval of 0.02 rad/s were considered in the analysis.

As can be seen from Figure 4, the first-order wave exciting force on surge gradually increases with the increase in the platform width (i.e., M1–M4). When the skirt width increases, the excitation force in surge becomes slightly larger (e.g., by comparing M4, M9, and M10). The increase in the compartment width and retaining wall width may result in a larger excitation force in surge at certain frequencies, as compared among M4–M8. Therefore, the present sensitivity study shows that smaller dimensions lead to less excitation force in surge that could further benefit the design of mooring system by introducing smaller loads. In addition, smaller dimensions can usually reduce the material cost for the manufacturing. Therefore, M1–M4 were considered as potential design candidates.

Furthermore, the natural period of pitch for the designed barge structure is recommended to be within the range of 9 to 16 s by DNV Recommended Practice (<https://www.dnv.com/>, accessed on 3 March 2022) DNVGL-RP-0286 [32]. The natural periods of different platforms for pitch at 0° are summarized in Table 3 for M1–M4. Considering that a smaller platform usually leads to more challenging stability conditions, the M4 platform was selected instead of M3. Figure 5 shows the frequency domain RAO of the M4 platform. It can be seen that the peak of RAO in the heave and pitch directions is achieved at frequencies of 0.56 rad/s and 0.42 rad/s, respectively. The coupled analyses in the time domain were further conducted based on the M4 barge platform.

**Table 3.** Natural periods of different platforms for pitch at 0° direction.

Model ID	Frequency (rad/s)	Periods (s)
M1	0.34	18.48
M2	0.38	16.53
M3	0.4	15.71
M4	0.42	14.96

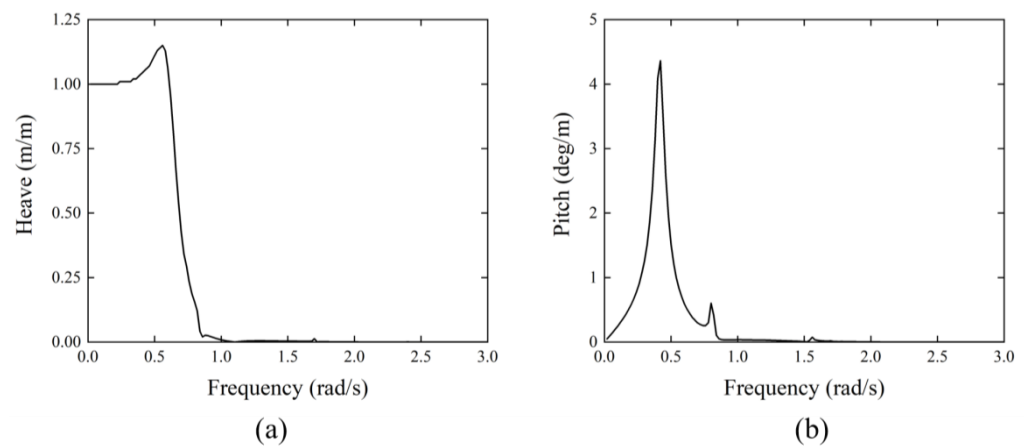


Figure 5. The RAO of (a) heave and (b) pitch in frequency domain.

For the M4 platform, the base of the turbine tower is located at (22 m, 0 m, 5 m). The center of gravity (COG) of the barge-type FOWT is located in the center of the moonpool at a height of 0.776 m above the stationary water level (SWL) during operation. The main geometrical information about the designed barge platform is summarized in Table 4. The platform dimensions, compartment structure, and mooring system are designed to align with the relevant requirements in DNVGL-RP-0286 [32] and DNVGL-OS-E301 [33].

Table 4. General specifications of the barge-type platform.

Parameter	Value
Barge dimensions (including skirt)	60 × 60 × 15 m
Moonpool dimension	14 × 14 m
Width of retaining walls	6 m
Compartment width	10 m
Skirt width	3 m
Draft	10 m
Barge COG	(−1.349 m, 0 m, −4.595 m)
Platform mass (including ballast)	20,371.539 t
Platform steel mass	4996.68 t
Displacement	21,112.20 m <sup>3</sup>

### 3.2. Mooring System

An eight-line catenary mooring system (4 × 2) was designed for the barge-type platform to keep it in position; the total length of each mooring line is 723.5 m. The mooring lines are split with four groups that spread symmetrically about the platform center with a 90-degree interval. The main properties are summarized in Table 5. The mooring system layout is indicated in Figure 6.

Table 5. Properties of the mooring lines.

Parameter	Value
Line type	Studless chain
Mooring line diameter	0.153 m
Mooring line length	723.5 m
Submerged weight per unit length	0.447 t/m
Radius to anchor from the platform centerline	735.23 m
Minimum breaking load	2.04 × 10 <sup>4</sup> kN
Axial stiffness	2.1 × 10 <sup>6</sup> kN
Pretension at fairlead	635.23 kN

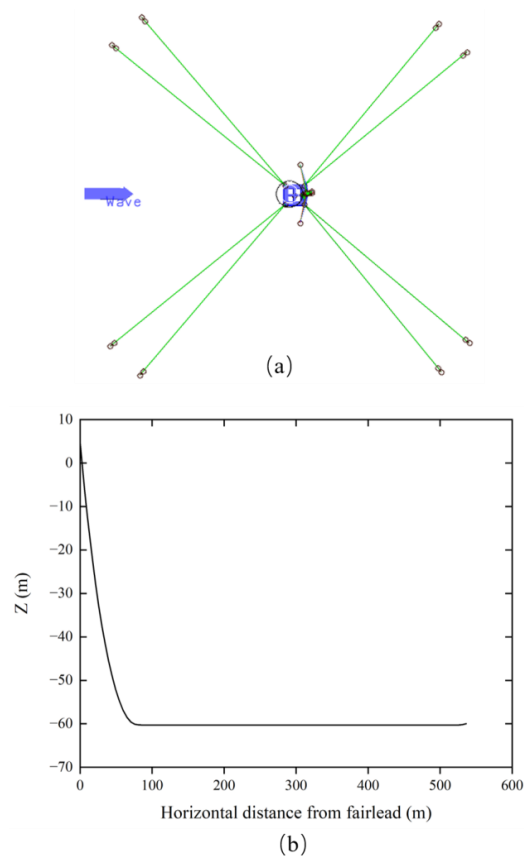


**Figure 6.** Illustration of the barge platform mooring system. (a) Layout of the mooring lines. (b) Configuration of a mooring line in the projected view.

#### 4. Stability Analysis

The HydroD-Wadam [34] module was used to analyze the intact and damage stability of the selected M4 platform. The stability of the FOWT was checked according to DNV-OS-C301 [35]. The wind-induced loads on the turbine reach the maximum at the rated wind speed. Consequently, the wind loads on the blades and tower at the rated wind speed were considered for the stability analysis. The following two requirements regarding the intact stability of the barge-type platform FOWT were considered [35]:

- (1) The area under the righting moment curve being equal to or greater than 140% of the area under the wind heeling moment curve for the inclination angles until the second intercept.
- (2) Over the entire range of angles from upright to the second intercept, the righting moment curve shall be positive.

For the damage stability check, each damaged condition only considered one broken compartment on the leeward side. Compartment damage on the leeward side is believed to be more critical as a result of the relatively large bending moment caused by the wind load, inclination of the tower, and water ingress of the compartment. The platform is designed to have 34 compartments from cm\_LC3\_c to cm\_LC36\_c, among which there are six main compartments on the leeward side, named cm\_LC27\_c to cm\_LC32\_c. DNV-OS-C301 requires that the barge-type platform as a ship-shaped unit shall: (1) have sufficient reserve stability for any of the considered damaged conditions; and (2) any down-flooding opening shall be above the waterline after flooding of the damaged compartment. At this stage of initial design of the barge platform, more stringent criteria with respect to the damage stability were considered:

- (1) The ratio of the max righting moment and heeling moment should be greater than 2.
- (2) The initial equilibrium inclination for the damaged condition should be less than  $17^\circ$

The results for the intact and damage stability checks are shown in Figure 7. It can be observed that the intact stability and damage stability of the M4 platform meets the specification requirements.

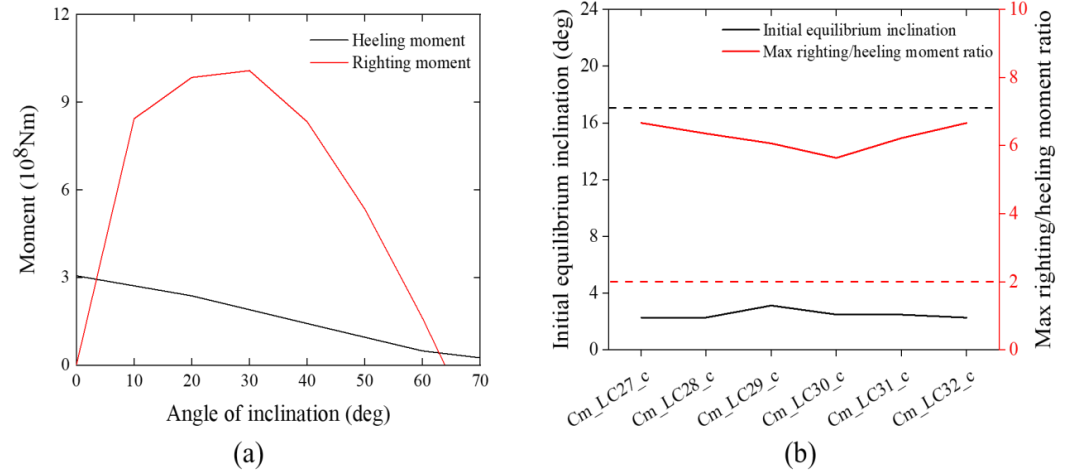


**Figure 7.** Stability analysis results. (a) The righting moment and heeling moment for intact stability check. (b) The ratio between the maximum ratio between the righting and heeling moments (red) and initial equilibrium inclination (black) for different damaged compartments.

Compared with the designed semi-submersible platform supporting the DTU 10 MW wind turbine [29], the intact stability-to-area ratio of the barge platform was 3.66, which was 2.61 times that of the semi-submersible platform, indicating the significantly better intact stability of the barge platform.

**5. Coupled Time Domain Analysis**

The structural responses of the blades, tower, platform, and the mooring lines were calculated in the time domain using SIMA software. The coupling among wind loads, wave loads, and structural dynamics are handled by SIMA Simo-Riflex-AeroDyn (SRA) [36], where the structural hydrodynamics is considered through Simo and Riflex, whereas the aerodynamics of turbine blades is considered through AeroDyn. Bachynski [37] described the procedure of applying SRA for coupled dynamic analysis, as briefly illustrated in Figure 8.

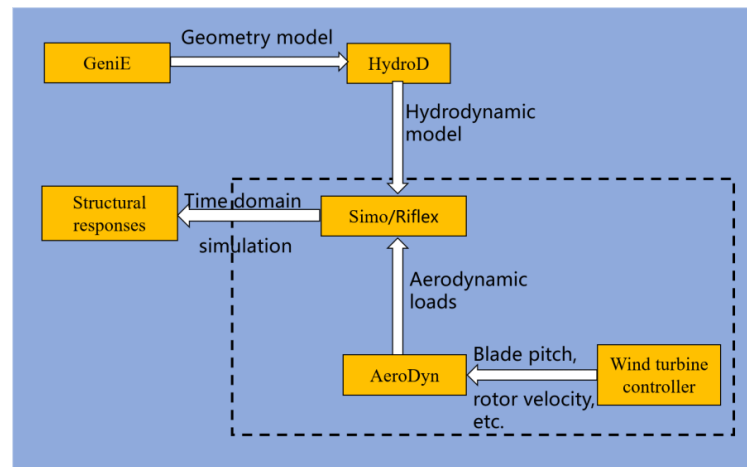


**Figure 8.** Coupling analysis in SESAM and SIMA.

Coupled time domain simulations were carried out to study the dynamics of the barge-type FOWT system with the mooring system under the actions of wind and waves.

The decay analyses were also performed in the time domain using the coupled dynamic analysis approach to evaluate the platform natural periods.

### 5.1. Free Decay Tests

Numerical simulations for free decays in six DoFs were conducted in SRA to obtain the nature periods of the proposed barge-type FOWT. The wind turbine was assumed to be parked with all blades fastened in the decay tests. For each DoF, an excitation (force or moment) was applied on the COG of the barge-type FOWT for 10 s in order to provide an initial offset at the corresponding DoF. This excitation was then removed in the simulation so that the FOWT started oscillating freely and decaying.

The moonpools introduce resonance (e.g., piston and sloshing modes) at certain critical periods which can amplify the response of the platform. Usually, we can reduce the resonance amplitude by providing additional viscous drag damping through installing various structures (e.g., cofferdam, plates, etc.) inside the moonpools.

However, the important nonlinear damping due to viscosity cannot be calculated by HydroD based on linear potential theory. It is usually acceptable to include an additional 5% to 8% critical damping [38]. Considering that the platform is equipped with skirts and assuming certain measures can be taken to increase the moonpool damping, 8% critical damping was added to the HydroD model as the viscous damping.

The time series of surge, heave, pitch, and yaw motions for the decay tests are illustrated in Figure 9. Due to symmetry of the barge-type platform, sway and roll responses are similar to surge and pitch. As indicated in Table 6, the mean natural periods in surge, heave, pitch, and yaw for the proposed M4 platform obtained from the decay simulations are well within the recommended ranges in DNVGL-RP-0286.

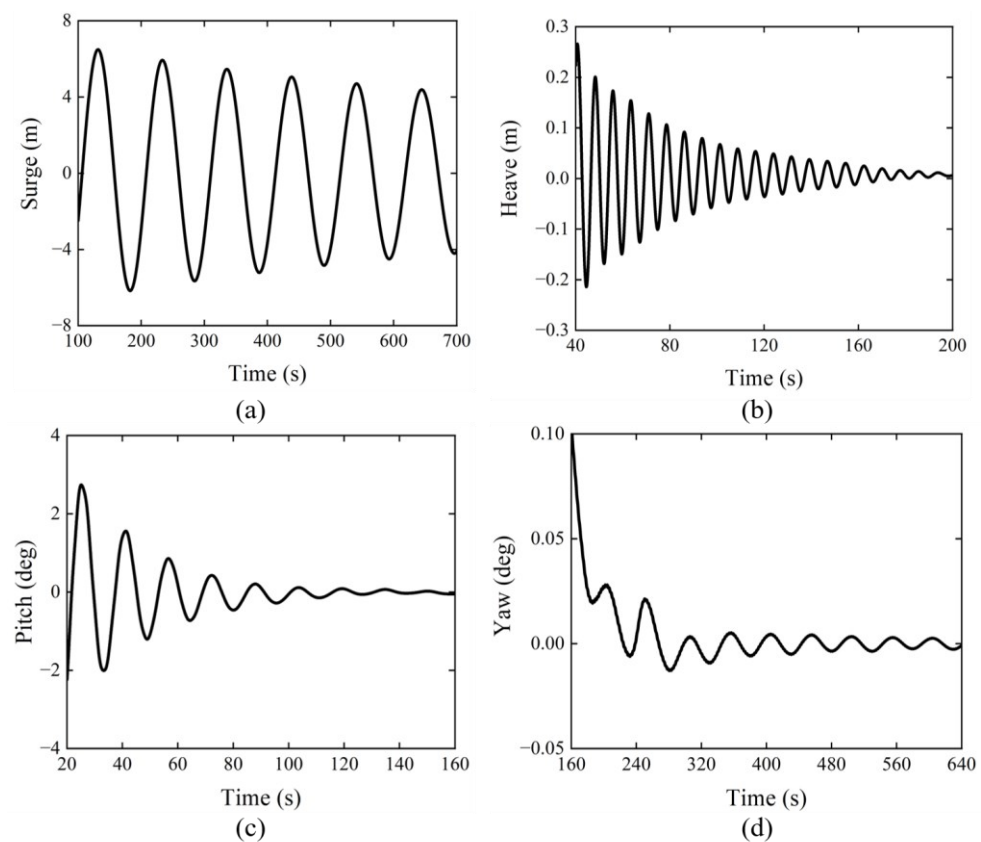


Figure 9. Platform response time series of (a) surge, (b) heave, (c) pitch, and (d) yaw in decay tests.

**Table 6.** Natural periods of barge platform.

DoF	Natural Periods [s]	
	Simulated	Recommended
Surge/Sway	103.09	~100
Heave	7.62	5–10
Pitch/Roll	15.67	9–16
Yaw	52.91	50–100

5.2. Environmental Conditions

The dynamic behavior of the proposed barge-type FOWT was evaluated under combined wind and wave loads for parked and operating wind turbine status. The environmental conditions were determined according to IEC 61400-3 [39]. Turbulent wind was considered using the IEC Kaimal model [40] with turbulence level C simulated by the TurbSim [41]. JONSWAP wave spectra were applied to represent the sea states. The details of the considered 18 load cases (LCs) are shown in Table 7. LC1–LC6 are the extreme environmental conditions with a 50-year return period when the wind speed exceeds the cut-out wind speed. Therefore, the wind turbine is in a parked state for LC1–LC6 and the blade pitch angle is 90°. LC7–LC12 are the environmental conditions with a 5-year return period, and LC13–LC18 are the combination of sea states and wind with a 2-year return period. The wind turbine is in operation for LC7–LC18 when the wind speeds are less than the cut-out wind speed. Wave and wind directions between 0° and 225° were considered with a 45° interval. Under operating conditions, the nacelle yaw rotates to face the wind in line with the direction of the incoming wave and wind so that the blades can fully capture the wind energy. The present study conservatively assumed that the wind and waves are in the same direction.

**Table 7.** The main characteristics of the wind and wave conditions for the considered load cases.

Load Case ID	Return Period (Year)	H <sub>S</sub> (m)	T <sub>P</sub> (s)	V <sub>Hub</sub> (m/s)	Direction (°)	Turbine Status
LC1	50	8.96	13.50	34.16	0	Parked
LC2		8.45	10.40	36.78	45	
LC3		8.13	9.30	40.05	90	
LC4		8.69	16.40	35.55	135	
LC5		10.16	13.80	49.01	180	
LC6		9.07	11.50	37.79	225	
LC7	5	5.10	11.10	20.77	0	Operating
LC8		6.21	9.80	24.92	45	
LC9		5.94	8.20	24.96	90	
LC10		5.47	13.60	23.37	135	
LC11		4.99	12.20	20.15	180	
LC12		6.42	10.00	24.82	225	
LC13	2	3.50	10.80	15.22	0	Operating
LC14		4.22	8.70	19.17	45	
LC15		3.68	7.00	17.40	90	
LC16		4.34	12.20	18.76	135	
LC17		3.81	10.40	15.64	180	
LC18		4.11	8.30	18.79	225	

5.3. Comparative Analysis of Different Mooring System Designs

The proposed mooring system of the barge-type FOWT is made up of eight catenary chains that are evenly divided into four groups. Among a vast number of possible mooring systems that may be suitable for typical FOWTs (e.g., [42]), an alternative may be made up of nine catenary chains evenly divided into three groups as proposed by IDEOL [43]. The layouts of the two mooring system designs are displayed in Figure 10. It is of interest to

compare the influence of these two mooring systems on the response of the platform and the mooring lines themselves. To ensure the comparability of different mooring system designs for the barge-type FOWT, the mechanical properties of the mooring lines (e.g., the axial stiffness, diameter, submerged mass, etc.) remain the same. The layout (i.e., the layback distance) was adjusted so that the surge resonance period from the decay test remains approximately the same.

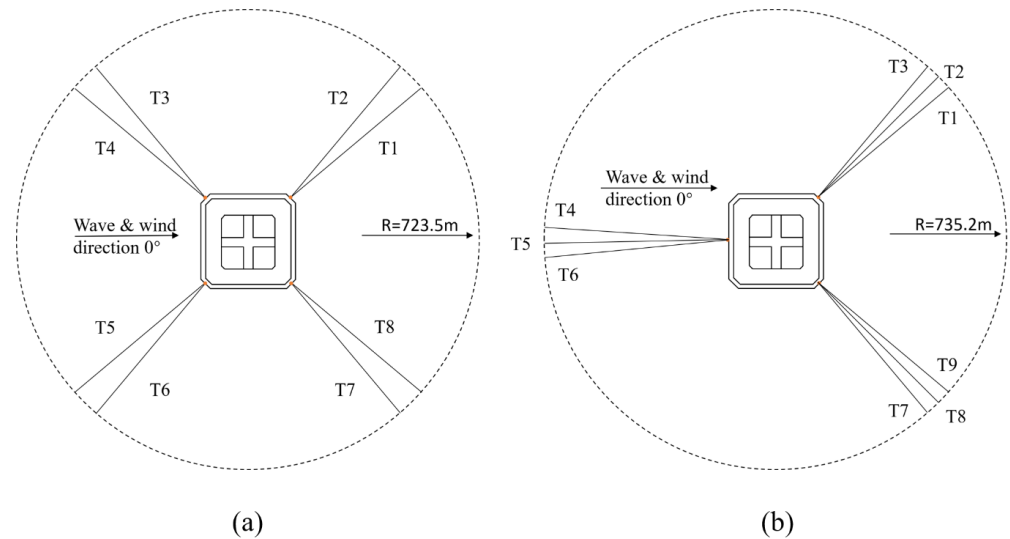


Figure 10. Illustration of mooring systems: (a) 4 × 2 mooring system; (b) 3 × 3 mooring system.

The barge-type FOWT response and the mooring line tension with two different mooring system designs were simulated and compared for LC1, LC2, and LC13. Each simulation lasts for 4800 s. The first 1200 s time series were taken out to remove the startup transient effects.

The time series of the surge, heave, and pitch motions and the maximum mooring line tensions in the two mooring systems are presented in Figures 11 and 12 for LC1 and LC13, respectively. The difference in the mooring system has little effect on the consequent platform heave and pitch response for LC1 and LC13. In terms of mooring line tension, the difference in the surge motions and the top tensions of the critical mooring lines for the two mooring systems are not extremely significant. As shown in Table 8, for LC2, the maximum surge motions of the two mooring systems are similar. However, the maximum sway for the 3 × 3 mooring system is significantly greater than that for the 4 × 2 mooring system due to the asymmetry environmental loading for the platform with the 3 × 3 mooring system for the wind and wave direction of 45°. Consequently, the maximum mooring tensions for the two mooring systems are also different. The maximum tension of the critical mooring line for both mooring systems is marginally less than the minimum breaking load, satisfying the relevant design requirement. Therefore, from an economic point of view, the 4 × 2 mooring system is selected for the proposed barge-type FOWT instead of the 3 × 3 mooring system.

Table 8. The motion response comparison.

Parameter	4 × 2 Mooring System	3 × 3 Mooring System
Maximum surge (m)	6.42	6.24
Maximum sway (m)	6.45	12.03
Maximum mooring tension (kN)	3201.59	2152.00

5.4. Influences of Wind and Wave Loads on the Barge-Type FOWT Dynamics

The maximum absolute (max. abs.) value, mean, and standard deviation (STD) of the six DoFs motions of the platform from LC1 to LC18 are illustrated in Figure 13. Figure 13a shows that the platform surge motion amplitude can be very significant under the parked condition. The maximum absolute value of 18.03 m surge is obtained at the 50-year return period condition LC5 for the wind and wave direction of 180° with the largest wind speed and wave height. The maximum absolute value of sway motion occurs in LC6.

The heave response of the wind turbine in the operating state is much smaller than that under the extreme weather with parked conditions. The main reason is that the large wave amplitude in the parked condition results in an increase in the amplitude of the heave motion. In general, in terms of surge, sway, and heave motions, the motion response of the platform under the parked conditions is more significant than those under the operating conditions. Due to rotor gyro effect, the yaw motions of the barge platform in the operation conditions are larger than those in the parked state. The maximum absolute yaw motion is 9.22° from LC15.

According to the DNV-RP-0286 [32], the maximum allowable inclination angle of the FOWT is 15° for the non-operational load cases and 10° for the operating conditions. The maximum absolute value of roll motion is 9.25° from LC4. Whereas the largest pitch motion is greater than 10° for LC1 and LC5 under the parked state, which is less than the allowed inclination angle of 15°. The initially designed barge platform satisfies the relevant preliminary requirements recommended by DNV.

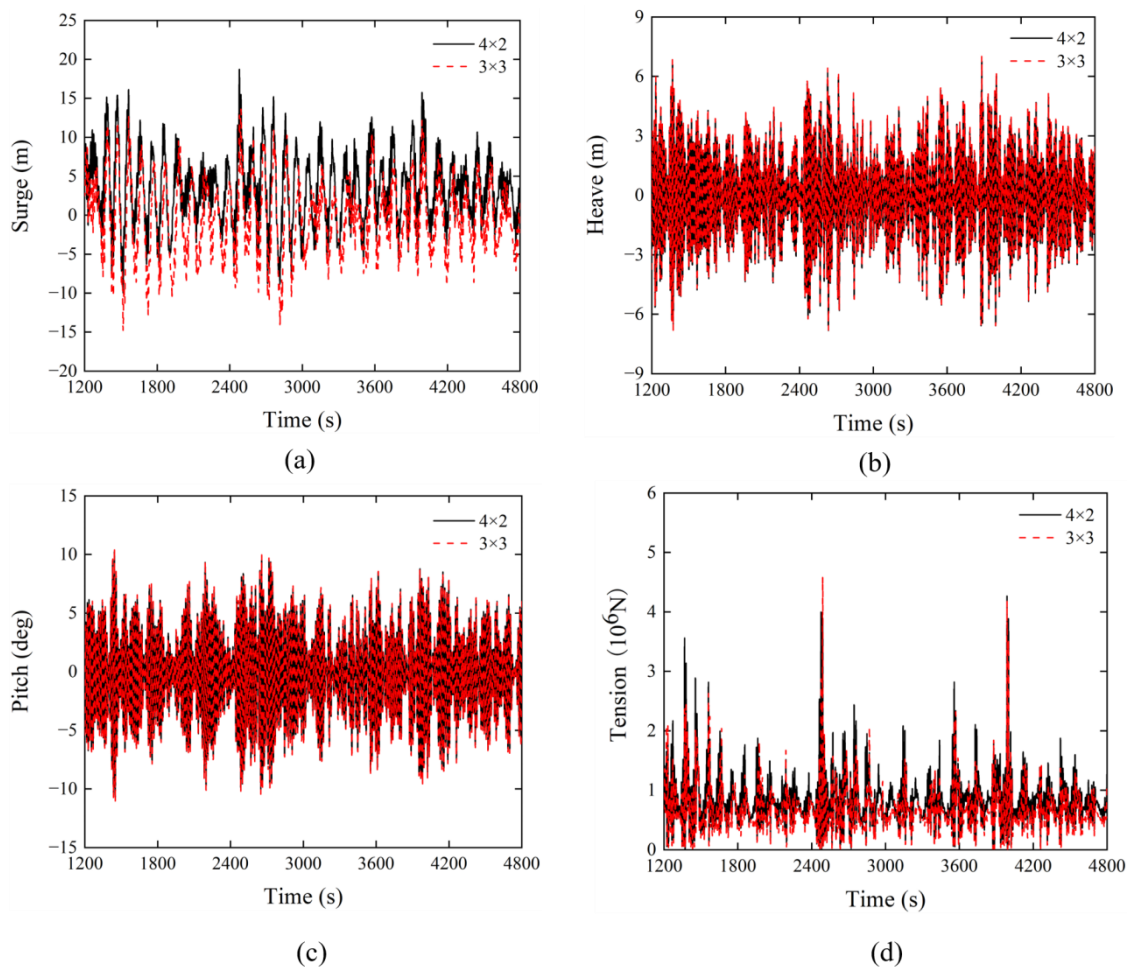
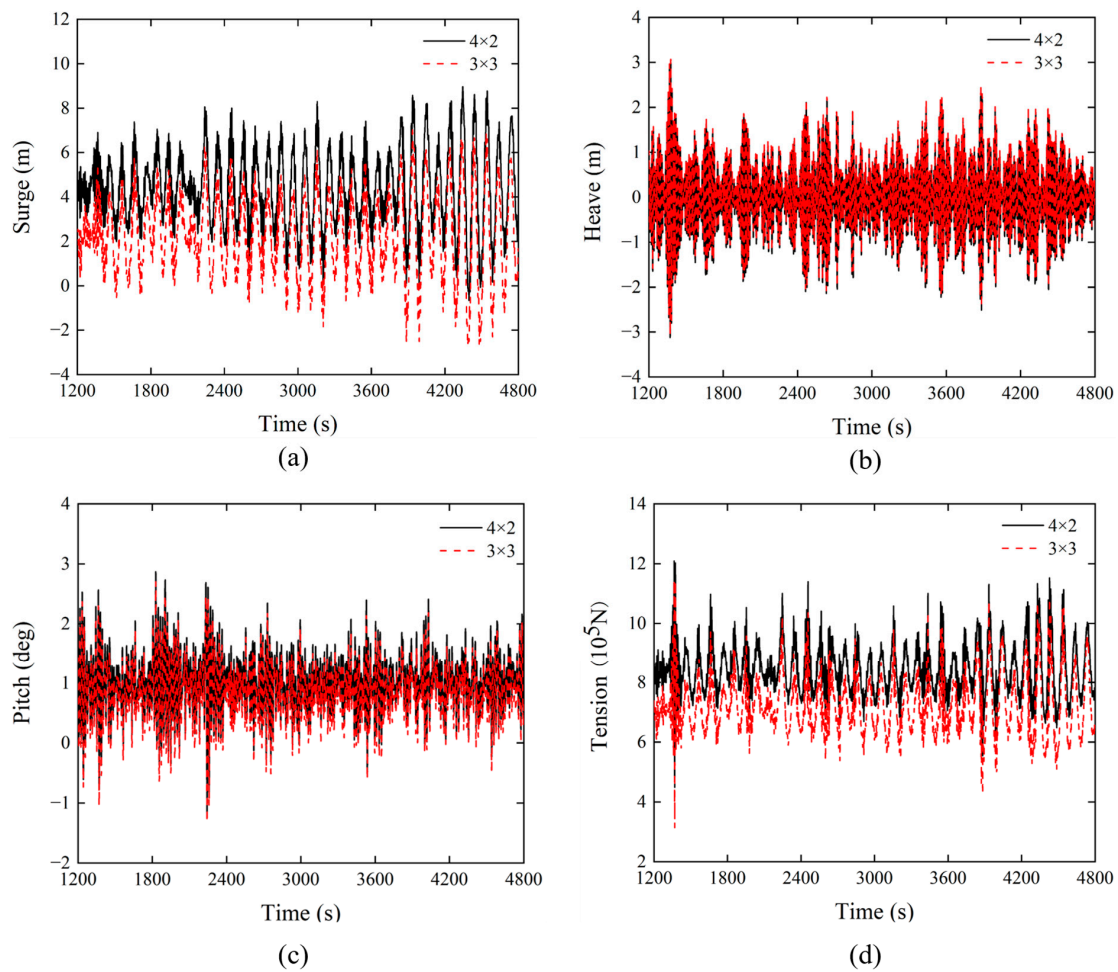


Figure 11. Comparison of (a) surge, (b) heave, (c) pitch, and (d) top tension of mooring line T5 in the 4 × 2 system and mooring line T6 in the 3 × 3 system for LC1.



**Figure 12.** Comparison of (a) surge, (b) heave, (c) pitch, and (d) top tension of mooring line T5 in the  $4 \times 2$  system and mooring line T6 in the  $3 \times 3$  system for LC13.

The calculation results of the maximum absolute, mean, and STD of the side-to-side (S-S) and fore-aft (F-A) bending moments at the base tower from LC1 to LC18 are demonstrated in Figure 14. It can be seen that the tower-base F-A bending moment amplitude is much larger than the tower-base S-S bending moment when the wind and waves propagate in the  $x$ -axis direction. The tower-base F-A bending moment is the largest when the angle of the wind and waves is  $180^\circ$  under the 50-year return period conditions. However, when the wind and wave propagate along the  $y$ -axis, the tower-base F-A bending moment is smaller than that of the tower-base S-S bending moment. It can also be seen from Figure 14 that the tower-base S-S bending moment is significantly smaller when the wind and waves propagate in the  $x$ -axis direction, compared with other environmental directions. The extreme value of the tower-base bending moment under the 50-year return period environmental conditions is much greater than that under the 5-year and 2-year encounter conditions. The maximum absolute value of the tower-base F-A and S-S bending moments are  $8.72 \times 10^8$  Nm and  $6.46 \times 10^8$  Nm, occurring in LC5 along  $180^\circ$  and LC4 along  $135^\circ$ , respectively.

Based on the symmetricity of the proposed  $4 \times 2$  mooring system, statistical results of the dynamic analyses for the mooring lines T1, T3, T5, and T7 (as illustrated in Figure 10) are reported for load cases LC1–LC18, as shown in Figure 15. The tension of mooring line T1 reaches the largest (i.e., 5634.3 kN) at the parked condition with  $180^\circ$  wave direction. The parked condition generally led to a more critical response for the mooring lines due to the exposed onerous environmental conditions compared with the operating conditions. Therefore, as expected, the tension STDs for the conditions with 50-year return period are

greater than those with 5-year and 2-year return periods. Furthermore, the largest top tension in T7 is 4729.4 kN, occurring in LC6. The maximum mooring line tension of the mooring lines T3 and T5 is obtained in LC2 and LC1, respectively.

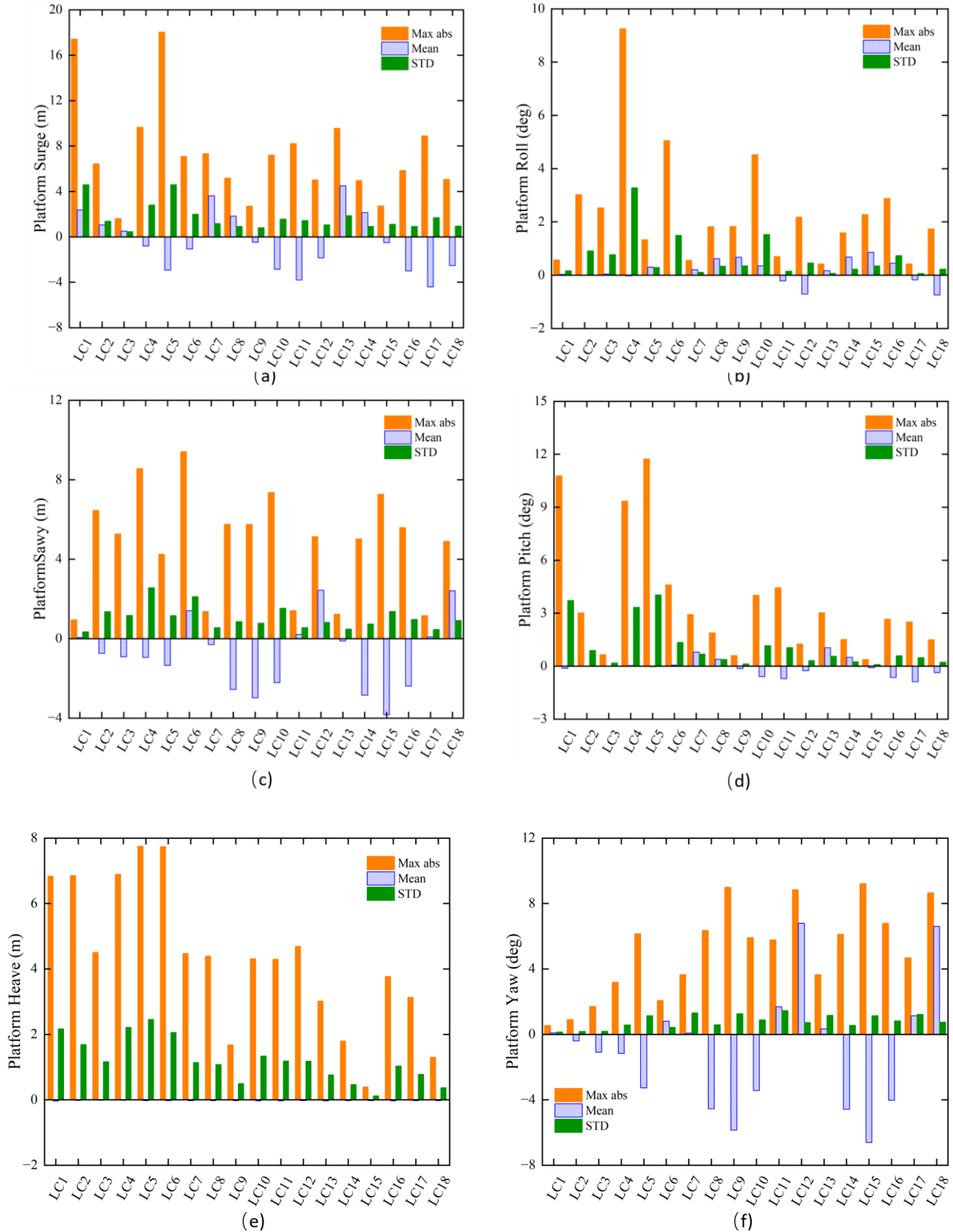


**Figure 13.** Statistics of the platform motion response for (a) surge, (b) roll, (c) sway, (d) pitch, (e) heave, and (f) yaw for all the considered load cases.

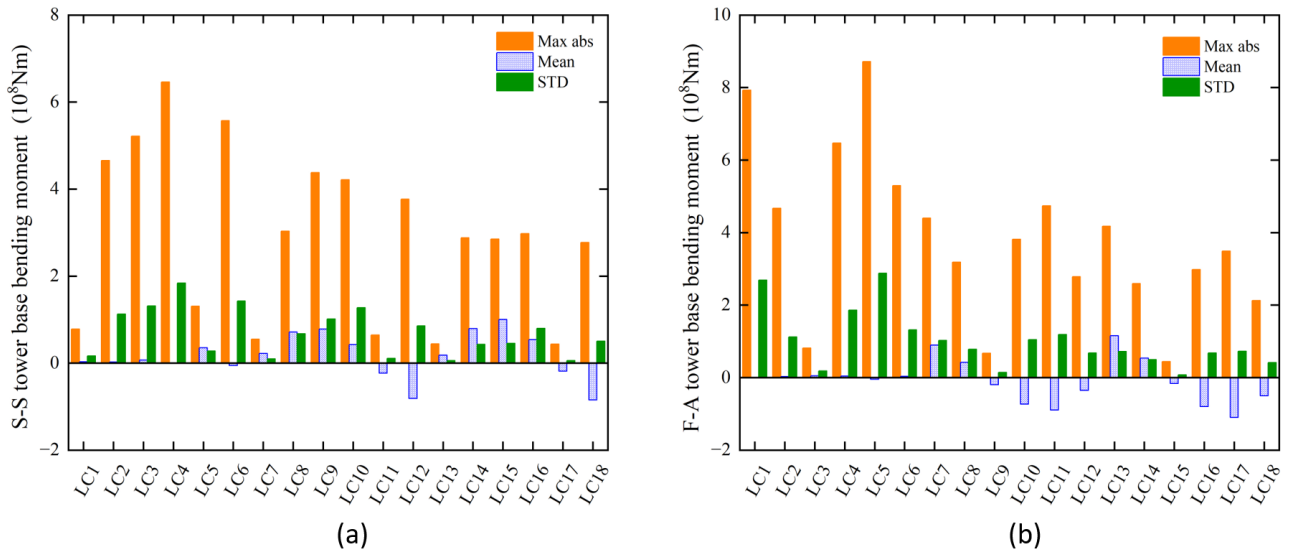


Figure 14. The bending moment of (a) S-S tower base, (b) F-A tower base for all the considered load cases.

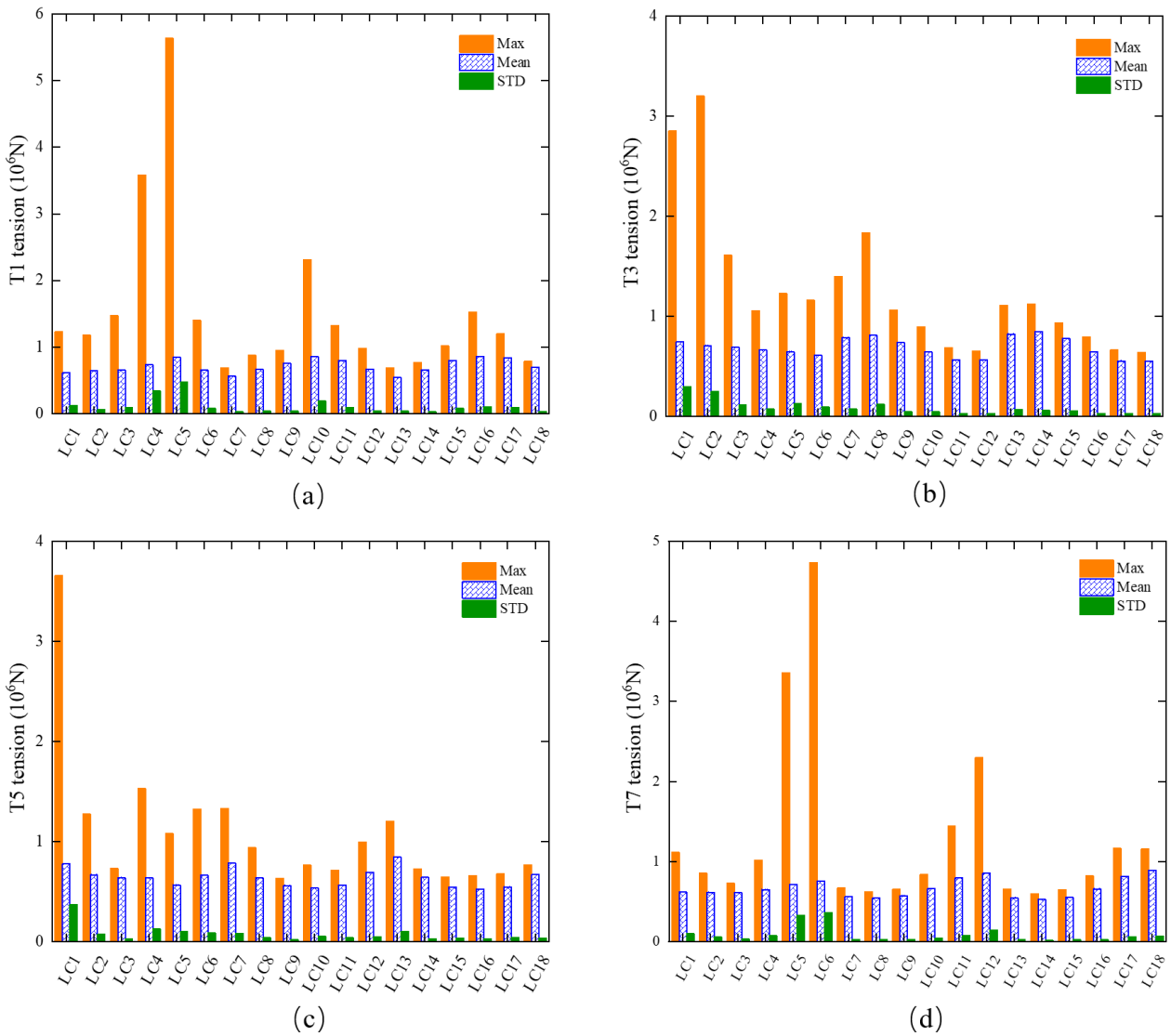


Figure 15. Statistics of mooring line top tension for (a) T1, (b) T3, (c) T5, and (d) T7.

## 6. Conclusions and Future Work

This paper proposes a new concept for a barge platform supporting the DTU 10 MW wind turbine. The key geometrical dimensions of the barge platform are determined based on the excitation load in surge and the natural pitch period at  $0^\circ$  calculated by HydroD, comparing 10 barge platforms with different sizes. The barge-type FOWT satisfies the requirements with respect to the intact stability and damage stability according to DNV-OS-C301. Furthermore, the  $4 \times 2$  mooring system is proposed. Its dynamic performance has been compared with the  $3 \times 3$  mooring system. Many coupled analyses have been conducted to simulate the dynamic responses of the barge-type FOWT by using SIMA with various operational and environmental conditions. The main conclusions regarding the initial design of the barge-type FOWT drawn from the study can be summarized as follows:

- (1) The newly designed barge FOWT system is proven to have reasonably good stability. Its six DoF natural periods and intact and damage stability meet the relevant DNV recommendations.
- (2) The difference in the dynamic response of the barge FOWT with the  $4 \times 2$  and the  $3 \times 3$  mooring system design is not very significant. Therefore, the  $4 \times 2$  mooring system design is chosen from an economic point of view. The maximum mooring line tension is 5634.3 kN, which is sufficiently smaller than the breaking load of the mooring lines.
- (3) The platform motions under the considered 18 load cases are also studied. The motion responses of the integrated barge-type FOWT system are within reasonable ranges. Particularly, the largest pitch and roll responses are demonstrated to be acceptable based on the limited scope of simulations.

In the future, the initially designed barge platform should be further comprehensively checked against the relevant standards by:

- (1) Considering more complete environmental conditions (e.g., including current effects);
- (2) Checking that the critical structural responses against the ultimate strengths of relevant materials;
- (3) Ensuring that the platform meets the design life through fatigue assessment;
- (4) Checking the proposed mooring system can well function with the failure of an arbitrary mooring line;
- (5) Ensuring the design of turbine and blades meeting the relevant standards.

Furthermore, due to the expected complexity of the dynamic analysis involving four moonpools, the numerical simulations for the dynamics of the proposed barge-type FOWT should be preferably validated by model-scale tests. In addition, the application of barge-type platforms for a larger wind turbine (e.g., the IEA 15 MW reference turbine) should be considered so as to follow the offshore wind development trend for increasing wind turbine size to reduce the electricity cost. Last but not at least, the significant capacity margin regarding the ultimate tensile strength for the mooring lines indicates that there can be a significant potential for mooring system optimization with respect to, e.g., arrangement, cross sectional dimension, and material.

**Author Contributions:** Conceptualization, Y.Z. and X.H.; methodology, Y.Z., W.S. and S.F.; software, S.F. and Y.Z.; formal analysis, S.F.; investigation, X.G. and X.L.; resources, Y.Z. and F.T.; writing—original draft preparation, Y.Z. and S.F.; writing—review and editing, Y.Z., S.F., X.H., W.S., and F.T. All authors have read and agreed to the published version of the manuscript.

**Funding:** This research was funded by the China Huaneng Group Science and Technology Fund (HNKJ20-H53) and the National Natural Science Foundation of China (Grant No. 52071058, 51939002). This work is also partially supported by special funds for promoting high quality development from the Department of Natural Resources of Guangdong province (GDNRC [2020]016), the Central Guidance on Local Science and Technology Development Fund of Shenzhen (2021Szvup018), and the Fundamental Research Funds for the Central Universities (DUT22RC(3)069).

**Institutional Review Board Statement:** Not applicable.

**Informed Consent Statement:** Not applicable.

**Data Availability Statement:** Not applicable.

**Conflicts of Interest:** The authors declare no conflict of interest.

## References

- Shi, W.; Zhang, L.; Karimirad, M.; Michailides, C.; Jiang, Z.; Li, X. Combined effects of aerodynamic and second-order hydrodynamic loads for three semisubmersible floating wind turbines in different water depths. *Appl. Ocean Res.* **2023**, *130*, 103416. [CrossRef]
- U.S. Department of Energy DOE. *20% Wind Energy by 2030: Increasing Wind Energy's Contribution to U.S. Electricity Supply; Executive Summary*. U.S. Department of Energy: United States, 2008. Available online: <https://www.energy.gov/eere/wind/articles/20-wind-energy-2030-increasing-wind-energys-contribution-us-electricity-supply-0> (accessed on 17 March 2022).
- Barthelmie, R.J.; Pryor, S.C. Climate Change Mitigation Potential of Wind Energy. *Climate* **2021**, *9*, 136. [CrossRef]
- Shi, W.; Zeng, X.; Feng, X.; Shao, Y.; Li, X. Numerical study of higher-harmonic wave loads and runup on monopiles with and without ice-breaking cones based on a phase-inversion method. *Ocean Eng.* **2023**, *267*, 113221. [CrossRef]
- Chen, J.; Pei, A. A Review of the Key Technologies for Floating Offshore Wind Turbines. *South Energy Constr.* **2020**, *7*, 8–20. (In Chinese)
- Zhang, L.; Shi, W.; Zeng, Y.; Michailides, C.; Zheng, S.; Li, Y. Experimental investigation on the hydrodynamic effects of heave plates used in floating offshore wind turbines. *Ocean Eng.* **2023**, *267*, 113103. [CrossRef]
- Jonkman, J.M. *Dynamics Modeling and Loads Analysis of an Offshore Floating Wind Turbine*; Technical Report NREL/TP-500-41958; University of Colorado: Boulder, CO, USA, 2007.
- Wayman, E.N.; Sclavounos, P.D.; Butterfield, S.; Jonkman, J.; Musial, W. Coupled Dynamic Modeling of Floating Wind Turbine Systems. In Proceedings of the 2006 Offshore Technology Conference, Houston, TX, USA, 1–4 May 2006.
- Jonkman, J.M.; Buhl, M.L. Loads Analysis of a Floating Offshore Wind Turbine Using Fully Coupled Simulation. In Proceedings of the Wind Power 2007 Conference and Exhibition, Los Angeles, CA, USA, 3–6 June 2007.
- Jonkman, J.; Matha, D. A Quantitative Comparison of the Responses of Three Floating Platforms. In Proceedings of the European Offshore Wind 2009 Conference and Exhibition, Stockholm, Sweden, 14–16 September 2009.
- Zhao, Z.; Shi, W.; Wang, W.; Qi, S.; Li, X. Dynamic Analysis of a Novel Semi-submersible Platform for a 10 MW Wind Turbine in Intermediate Water Depth. *Ocean Eng.* **2021**, *237*, 109688. [CrossRef]
- Ren, Y.; Venugopal, V.; Shi, W. Dynamic Analysis of a Multi-column TLP Floating Offshore Wind Turbine with Tendon Failure Scenario. *Ocean Eng.* **2022**, *245*, 110472. [CrossRef]
- Mayilvahanan, A.; Selvam, P.R. Time Domain Response Analysis of Barge Floater Supporting an Offshore Wind Turbine. *Int. J. Ocean Clim. Syst.* **2011**, *2*, 303–314. [CrossRef]
- Bossler, A. *Floating Offshore Wind Foundations: Industry Consortia and Projects in the United States. Europe and Japan*, Maine International Consulting LLC. 2013. Available online: <https://1library.net/document/qm6v837y-floating-offshore-foundations-industry-consortia-projects-pro> (accessed on 19 March 2022).
- Borisade, F.; Choisnet, T.; Cheng, P.W. Design Study and Full Scale MBS-CFD Simulation of the IDEOL Floating Offshore Wind Turbine Foundation. *J. Phys.* **2016**, *753*, 92002. [CrossRef]
- Guignier, L.; Courbois, A.; Mariani, R.; Choisnet, T. Multibody Modelling of Floating Offshore Wind Turbine Foundation for Global Loads Analysis. In Proceedings of the Twenty-Sixth (2016) International Ocean and Polar Engineering Conference, Rhodes, Greece, 26 June–1 July 2016.
- Choisnet, T.; Geschier, B.; Vetrano, G. Initial Comparison of Concrete and Steel Hulls in the Case of IDEOL'S Square Ring Floating Substructure, WWEC 2016. Available online: <https://www.researchgate.net/publication/335727818> (accessed on 24 March 2022).
- Kosasih, K.M.A.; Niizato, H.; Okubo, S.; Mitani, S.; Suzuki, H. Wave Tank Experiment and Coupled Simulation Analysis of Barge-Type Offshore Wind Turbine. In Proceedings of the 29th International Society of Offshore and Polar Engineering Conference (ISOPE-2019), Hawaii, HI, USA, 16–21 June 2019.
- Vijay, K.G.; Karmakar, D.; Uzunoglu, E.; Soares, C.G. Performance of Barge-Type Floaters for Floating Wind Turbine. In Proceedings of the 2nd International Conference of Renewable Energies Offshore (Renew 2016), Lisbon, Portugal, 24–26 October 2016.
- Ikoma, T.; Nakamura, M.; Moritsu, S.; Aida, Y.; Masuda, K.E.H. Effects of Four Moon Pools on a Floating System Installed with Twin-VAWTs. In Proceedings of the ASME 2019 2nd International Offshore Wind Technical Conference, St. Julian's, Malta, 3–6 November 2019.
- Ikoma, T.; Tan, L.; Moritsu, S.; Aida, Y.; Masuda, K. Motion Characteristics of a Barge-type Floating Vertical-axis Wind Turbine with Moonpools. *Ocean Eng.* **2021**, *230*, 109006. [CrossRef]
- Sintef Ocean. SIMA Documentation. Available online: <https://sima.sintef.no/doc/4.4.0/sima/index.html> (accessed on 21 May 2022).
- Manwell, J.F.; McCowan, J.G.; Rogers, A.L. *Wind Energy Explained: Theory, Design and Application*; John Wiley & Sons: New York, NY, USA, 2002.
- Zeng, Y.; Shi, W.; Ren, Z.; Li, X. Turbulence Model Effects on the Hydrodynamic Response of an Oscillating Water Column (OWC) with Use of a Computational Fluid Dynamics Model. *Energy* **2022**, *261*, 124926. [CrossRef]

25. Greco, M. *Lecture Notes to TMR 4215: Sea Loads*; Department of Marine Technology, Norwegian University of Science and Technology: Trondheim, Norway, 2012.
26. Craig, R.R.; Kurdila, A.J. *Fundamentals of Structural Dynamics*, 2nd ed.; John Wiley: Hoboken, NJ, USA, 2006; pp. 13–78.
27. Naess, A.; Moan, T. *Stochastic Dynamics of Marine Structures*; Cambridge University Press: Cambridge, UK, 2012.
28. Bak, C.; Zahle, F.; Bitsche, R.; Kim, T.; Yde, A.; Henriksen, L.C.; Natarajan, A.; Hansen, M.H. *Description of the DTU 10 MW Reference Wind Turbine*; DTU Wind Energy Report-I-0092; Technical University of Denmark: Roskilde, Denmark, 2013.
29. Wang, Q. *Design and Dynamic Analysis of a Steel Pontoon-Type Semi-Submersible Floater Supporting the DTU 10MW Reference Turbine*; Norwegian University of Science and Technology: Trondheim, Norway, 2014.
30. Musial, W.; Butterfield, S.; Ram, B. Energy from Offshore Wind: Preprint. Available online: <https://www.nrel.gov/docs/fy06osti/39450.pdf> (accessed on 2 February 2023).
31. DNV. *SESAM User Manual, HydroD V6.1.02. Wave Load & Stability Analysis of Fixed and Floating Structures*; DNV: Høvik, Norway, 2022.
32. DNV. *DNVGL-RP-0286 Coupled Analysis of Floating Wind Turbines*; DNV: Høvik, Norway, 2019.
33. DNV. *DNVGL-OS-E301 Position Mooring*; DNV: Høvik, Norway, 2015.
34. DNV. *Wadam User Manual, Wadam V10.1.03. Wave Analysis by Diffraction and Morison Theory*; DNV: Høvik, Norway, 2022.
35. DNV. *DNVGL-OS-C301 Stability and Watertight Integrity*; DNV: Høvik, Norway, 2020.
36. Ormberg, H.; Bachynski, E.E. Global analysis of floating wind turbines: Code development, model sensitivity and benchmark study. In Proceedings of the 22th International Offshore and Polar Engineering Conference, Rhodes, Greece, 17–23 June 2012.
37. Bachynski, E.E. Design and Dynamic Analysis of Tension Leg Platform Wind Turbines. Ph.D. Thesis, Norwegian University of Science and Technology, Trondheim, Norway, 2014.
38. Liu, Z. Comparative Hydrodynamic Performance Analysis of Three Typical Kinds of Semi-submersible Floating Foundation of Offshore Wind Turbines. Master's Thesis, South China University of Technology, Guangzhou, China, 2020.
39. IEC. *61400-3; Wind Turbines-Part 3: Design Requirements for Offshore Wind Turbines*. International Electrotechnical Commission: Geneva, Switzerland, 2009.
40. IEC. *61400-1; Wind Turbines-Part 1: Design Requirements for Offshore Wind Turbines*. International Electrotechnical Commission: Geneva, Switzerland, 2005.
41. Jonkman, J.; Buhl, J.M.L. *TurbSim User's Guide*; NREL/TP-500-39797. 2006. Available online: <https://www.nrel.gov/docs/fy06osti/39797.pdf> (accessed on 10 July 2022).
42. Xu, K.; Larsen, K.; Shao, Y.; Zhang, M.; Gao, Z.; Moan, T. Design and Comparative Analysis of Alternative Mooring Systems for Floating Wind Turbines in Shallow Water with Emphasis on Ultimate Limit State Design. *Ocean Eng.* **2021**, *219*, 108377. [CrossRef]
43. Kosasih, K.; Suzuki, H. Demonstration Experiment and Numerical Simulation Analysis of Full-Scale Barge-Type Floating Offshore Wind Turbine. *J. Mar. Sci. Eng.* **2020**, *8*, 880. [CrossRef]

**Disclaimer/Publisher's Note:** The statements, opinions and data contained in all publications are solely those of the individual author(s) and contributor(s) and not of MDPI and/or the editor(s). MDPI and/or the editor(s) disclaim responsibility for any injury to people or property resulting from any ideas, methods, instructions or products referred to in the content.